Egypt. J. Chem. **Vol. 65,** No. 3 pp. 39 - 49 (2022)

Egyptian Journal of Chemistry

http://ejchem.journals.ekb.eg/

Novel superparamagnetic nanocomposite of core-shell magnetic zeolite coated with chitosan crosslinked by glutaraldehyde: synthesis and characterization

Suyanta Suyanta*, Iip Izul Falah, Wahyu Nugroho, Kristiana Fajariatri, Mudasir Mudasir

** Department of Chemistry , Universitas Gadjah Mada Yogyakarta , INDONESIA*

Abstract

In the present study, a novel superparamagnetic nanocomposite composed of magnetite as the core and zeolite coated by glutaraldehyde-crosslinked chitosan as the shell has been successfully synthesized. The synthesis steps include coating silica on the surface of magnetite nanoparticles and conversion of the silica layer into a zeolite layer, coating of chitosan on the surface of the zeolite, and cross-linking reaction of chitosan using glutaraldehyde. The X-ray diffractogram has proven that the magnetite nanoparticles formed on the nanocomposite have a cubic structure. The formation of the minerals mordenite, clinoptilolite, and quartz on the magnetite surface is also confirmed. Infrared spectral analysis has revealed the existence of Fe–O–Si and Fe–O–Al bonds between magnetite and zeolite, and C=N bonds between chitosan and glutaraldehyde. The TEM image clearly shows that the resulting nanocomposite consists of zeolite-coated magnetite nanoparticles, which are incorporated in a glutaraldehyde crosslinked chitosan gel system. Measurements with ImageJ software suggest that the diameter of the composite is in the range of 20–75 nm, with an average diameter of 34.06 nm. Magnetic studies indicate that the nanocomposite is superparamagnetic with a saturation magnetization of 27.5 emu/g. Since the magnetite nanoparticles is positioned in the core of the composite, it is well protected from oxidation and therefore it is expected to have high magnetic stability. This magnetically separable nanocomposite is quite interesting and may be applied in the adsorption of heavy metal ions and cationic dyes from aquatic medium.

***Keywords*:** Magnetite; zeolite; chitosan; nanocomposite; superparamagnetic.

1. Introduction

Adsorption techniques using biopolymers are one of the most recommended processes for removing or reducing heavy metals from industrial wastewater, because of their economic and technical advantages [1, 2]. Chitosan is a superior bio-sorbent because of its capability to form complexes with various heavy metal ions [3, 4]. Chemically, chitosan is a linear chain of *β*-(1→4)-2-acetamido-2-deoxy-d-glucose, which has both amine ($–NH_2$) and hydroxyl (–OH) reactive groups. These reactive groups can participate in chemical reactions via the formation of metal chelates [5], making it capable to adsorb various heavy metal ions, such as Cu(II), Cd(II), Pb(II), Fe(III), Zn(II), and Cr(III) [6–8]. Chitosan has beneficial physicochemical properties, e.g. environment-friendly, non-toxic, biocompatible, biodegradable, bioactive, bio-absorbable, and anti-bacterial materials [9]. Recently, modified chitosan has also been used in many applications including biomedical and biomaterial applications [10, 11] as well as drug deliveries to enhance their efficacies [12, 13]. However, chitosan is susceptible to solubilization in acidic solution [14], leading to poor stability and difficulty in removing chitosan from aqueous medium when it is used as adsorbents. For these reasons, chitosan has been combined with some other materials, such as zeolite [15]. Ngah *et al*. [16] has reported zeolite composites with glutaraldehyde crosslinked chitosan to overcome the instability of chitosan in acetic acid, distilled water, and alkaline solution. Zeolite/chitosan composites exhibit good adsorption properties for various heavy metals [17–19] and are used as membranes for the elimination of As, Cd, Cr, and Pb ions [20]. The disadvantage of the zeolite/chitosan adsorbent in large-scale operations is that it tends to form a gel, which is difficult to be separated by using conventional separation methods, such as filtration, centrifugation, and decantation [21]. Some modifications have been made to solve this problem.

*Corresponding author e-mail: suyanta_mipa@ugm.ac.id (Suyanta Suyanta)

EJCHEM use only: Receive Date: 23 May 2021, Revise Date: 08 June 2021, Accept Date: 03 September 2021

DOI: 10.21608/ejchem.2021.54439.3777

For examples, previous studies [16–28] has modified the composites with magnetite (Fe_3O_4) so that it can be easily separated using a permanent magnetic field [25].

Although zeolite/chitosan composites have been widely used as adsorbents [26–29], the development of composites containing zeolite, chitosan, and magnetite is rarely reported. Therefore, the development of composites containing zeolite, chitosan, and magnetite is quite interesting and gives opportunity to further explore their possible use as magnetically separable adsorbents. Furthermore, it is well known that bald magnetite nanoparticles are easily oxidized to produce magnetically less material of Fe_2O_3 [30, 31], therefore magnetite should be placed as the core to protect it from oxidation. Several composites prepared from magnetite and natural zeolite have been previously reported [32-35], but none of them have concerned with the formation of a layered sphere composites where magnetite is placed in the core, while zeolite is as the shell (denoted as Fe_3O_4@Zeo). Meanwhile, most recently Deng et al [36] have successfully synthesized such material, but they do not use natural zeolites.

In this study, we report the first ever preparation of novel superparamagnetic nanocomposite composed of magnetite as the core and zeolite coated by glutaraldehyde-crosslinked chitosan as the shell. The synthesized was initiated by the preparation of Fe_3O_4@Zeo based on the previous procedure [36], i.e. coating silica on Fe_3O_4 nanoparticles (denoted as Fe_3O_4@SiO_2) and conversion of the silica layer to zeolite. The resulting Fe_3O_4@Zeo were then coated with chitosan via the hydrogen bonds [37]. The coated chitosan was crosslinked with glutaraldehyde (denoted as Chi-Glu-Chi) to increase the stability and adsorption capacity. The final product is magnetic zeolite core-shell nanocomposites coated with glutaraldehyde-crosslinked chitosan (hereafter denoted as Fe_3O_4@Zeo(Chi-Glu-Chi)). This composites is expected to have various active sites originating from zeolite and chitosan so that they can absorb more metal ions or cationic dyes through ion exchange and chelate formation. Moreover, the magnetite nanoparticles placed in the core of composite are much more protected from oxidation so that their magnetic properties can be longer preserved and therefore the composites are magnetically separable.

2. Experimental

Materials and Instrumentation

Chitosan was extracted from shrimp shells collected from the beach. All of the chemicals used were purchased from E. Merck (Germany), including $FeSO_4{\cdot}7H_2O$ (99+%), ethylene glycol (EG, Quality level: MQ100), glutaraldehyde (50 wt% in H_2O), HCl (37%), NaOH (100%), NH_4OH (27%), acetic acid (>99.9%), tetraethyl orthosilicate (TEOS, 99%), tetrapropylammonium hydroxide (TPAOH, 40 wt% aqueous solutions), poly(diallyl dimethylammonium chloride) (PDDA, 65 wt% in H_2O), triethylamine (99%), ethylenediamine (99%), acetone, and ethanol. All of those materials were analytical reagent grade and used without further purification. Nitrogen (N_2) gas was purchased from PT Samator Gas Industry, Yogyakarta, Indonesia. The distilled water and deoxygenated distilled water used in this experiment were produced by local laboratories.

The X-ray diffractograms were recorded on Shimadzu X-ray Diffractometer Model XD-3H, with Cu Kα powder irradiated at $\lambda = 0.15406$ nm. Infrared analysis was carried out by using Shimadzu FTIR-8010PC spectrometer. The FTIR spectra in the absorbance mode were recorded in the range of 4000–400 cm^{-1} at room temperature using the KBr disk technique. A transmission electron microscope (TEM JEM-3010) was employed to determine the morphology and size distribution of nanoparticles, in which the obtained images were processed using the ImageJ software. A vibrating sample magnetometer (VSM Oxford 1.2H) with magnetic fields of up to 20 kOe at room temperature was used to analyze the magnetic properties of the samples. Sonication was performed using the Ultrasonic Neytech 28H under ambient conditions.

Methods

Preparation of Fe_3O_4 nanospheres

The nanospheres of Fe_3O_4 were synthesized using the previously reported method [34]. $FeSO_4{\cdot}7H_2O$ (2.85 g), NaOH (4.25 g), and $NaNO_3$ (0.50 g) were dissolved in 25 ml of 1:1 EG/distilled water solution in a three-neck flask and heated to 70 ˚C. To expel oxygen, N_2 gas was bubbled into the solution. The solution was stirred for 2h and incubated for a day under an N_2 atmosphere. The solution of NaOH (1 M) was added into the flask until pH = 10, i.e. the optimum pH for magnetite formation. The mixture was then stirred again at 70 ˚C for 2 h to ensure the homogeneity of the solution and to complete reaction. The emergence of a black precipitate indicated the formation of Fe_3O_4 particles. The aqueous phase was decanted, and the sediment was washed thrice with deoxygenated distilled water. Finally, the Fe_3O_4 sediment was separated using a permanent magnet, dried under vacuum conditions at 50 ˚C for 5 h, and stored in desiccators.

Synthesis of the silicalite-1 zeolite seed

The silicalite-1 zeolite seed was synthesized using the procedure used by Dai *et al*. [39] with a little modification. TEOS (50 g) was mixed with TPAOH

solution (70 ml) and distilled water (50 g). After stirring for 12 h at 35 ˚C, the gel was transferred into a Teflon and crystallized for 3 days at 120 ˚C to yield a silicalite-1 zeolite seed gel.

Synthesis of Fe_3O_4@Zeo nanospheres

Firstly, Fe_3O_4@SiO_2 nanospheres were synthesized by the existing methods [40] with a little modification. Briefly, Fe_3O_4 nanospheres (1g) were treated in a solution of HCl (50 ml, 2 M) followed by ultrasonic vibration for 5 min. The Fe_3O_4 nanospheres were then magnetically separated and washed thoroughly with distilled water, and then dispersed in a mixture of distilled water (20 g), concentrated ammonia solution (1g, 28 Wt%), and ethanol (70 g) under ultra-sonication. Then, TEOS (5 g) was added to the dispersion while magnetically stirring and the reaction was allowed to continue for 12 h. The product was separated magnetically and washed with ethanol and distilled water, and then vacuum dried at 60 ˚C for 24 h.

Secondly, the layer of SiO_2 on Fe_3O_4@SiO_2 was converted to zeolite using the published procedure [36] with a little modification. The surfaces of Fe_3O_4@SiO_2 nanospheres were modified using PDDA (a cationic polyelectrolyte); then the negatively charged silicalite-1 zeolite seed nanoparticles and AlO_2^- was allowed to be adsorbed on PDDA surfaces by electrostatic interaction. The nanospheres were then heated at 140 ˚C in amine vapor to produce vapor phase transport (VPT). The silicalite-1 served as seeds for in situ growth, the layered amorphous SiO_2 in the Fe_3O_4@SiO_2 nanospheres served as a-Si "nutrition pool" [36], whereas AlO_2^- served as a source of Al in the zeolite structure [41]. In a typical synthesis, Fe_3O_4@SiO_2 nanospheres (5 g) was mixed with PDDA (2 g, Mw = 20.000 g/mol^{-1}) and distilled water (200 ml). The Fe_3O_4@SiO_2 nanospheres with adsorbed PDDA were magnetically separated and washed thrice in ammonia solution (1 M). The product was then re-dispersed in 100 ml aqueous dispersion containing silicalite-1 zeolite seed nanoparticles (1 g) and $NaAlO_2$ (2 g). The Fe_3O_4@SiO_2 nanospheres with adsorbed PDDA and AlO_2^-, and modified with silicalite-1 nanoparticles were magnetically separated and washed thrice in ammonia solution (1 M). The obtaining nanospheres were put in a porcelain crucible, and vacuum in a dry condition at a temperature of 30 ˚C. The crucible with the dried nanospheres powder was put in an autoclave (100 ml), where a liquid mixture of PDDA (0.4 g), ethylene diamine (0.1 g), and triethyl amine (2 g) is added first. Afterward, the autoclave was closed and heated in an oven at 140 ˚C for 72 h. Once cool, the product was washed with ethanol and then dried in a vacuum.

Preparation of chitosan

Chitosan was prepared according to a previously reported method [42] with a little modification, which includes deproteinization, demineralization, decolorization, and deacetylation. Shrimp shells were cleaned and washed thoroughly to remove any pollutants and ground to obtain a particle size of 40 mesh. Deproteination was performed by adding the NaOH solution (1 M, 500 ml) to the raw shrimp shells (50 g). The mixture was stirred at 65 ℃ for 1 h to complete the reaction and filtered. The resulting solid phase was washed thrice with distilled water and dried. Demineralization was performed by adding the HCl solution (1 M, 1:15 w/v) to the washed and dried solid phase. The mixture was stirred at 80 ℃ for 1.5 h to complete the reaction. After filtering and drying, the product of chitin was obtained and then converted into chitosan by decolorization and deacetylation. In the decolorization step, chitin was bleached using a solution of acetone/ethanol (1:1) at room temperature for 1 h and then filtered to produce the colorless chitin. For deacetylation step, the colorless chitin was mixed with a solution of 60% NaOH (1:10 w/v) and stirred at 90 ℃ for 2 h to form a slurry. Then, the slurry was filtered, washed thrice with distilled water, and dried to produce chitosan powder. The average deacetylation degree (DD%) was determined on the basis of the FTIR spectra according to the following formula [43]:

$$DD\% = 100 - [\frac{(A1655/A3450)}{1.33} \times 100],$$

Where A1655 is the absorbance at 1655 cm^{-1} of the amide I as a parameter of the *N*-acetyl group content, whereas A3450 is the absorbance at 3450 cm^{-1} of the internal standard, i.e. hydroxyl group. The ratio value of A1655 to A3450 equals to 1.33 indicates a perfectly acetylated chitin.

Synthesis of Fe_3O_4@Zeo(Chi-Glu-Chi)

Fe_3O_4@Zeo(Chi-Glu-Chi) was synthesized according to the published procedure [37], with a little modification. Fe_3O_4@Zeo composite (2 g) and chitosan (1 g) were mixed with the acetic acid solution (2%, 100 ml), stirred, and sonicated for 10 min. Then, the mixture was shaken for 30 min, and the glutaraldehyde solution (25%, 2 ml) was added. The product was sonicated for 60 min, in which the NH_4OH solution (25%) was added to adjust the pH up to 11 and sonicated again for 30 min. The mixture was incubated for 2 h, then the sediment was collected using an external magnet, washed with deoxygenated distilled water until the pH was near neutral (6.5–7.0), dried under vacuum conditions at a temperature of 60 ℃ for 12 h, and stored in desiccators. The FTIR, XRD, TEM, and VSM methods were used in the product characterization.

3. Results and discussion

X-Ray diffraction analysis

The X-ray diffractograms of as-synthesized Fe_3O_4,

Fe_3O_4@Zeo, chitosan, and Fe_3O_4@Zeo(Chi-Glu-Chi) are presented in Figure 1. Figure 1a shows some characteristic peaks for Fe_3O_4, i.e., 2θ = 30.27°, 35.70°, 43.40°, 54.3°, 57.42°, and 63.10°. These peaks match with the crystal plane of {2 2 0}, {3 1 1}, {4 0 0}, {4 2 2}, {5 1 1}, and {4 4 0}, respectively; which are in good accordance with the inverse cubic spinel phase of Fe_3O_4 (ICDD no. 85-1436) [44]. The peak intensities of the Fe_3O_4 sample are relatively high, indicating a high crystallinity.

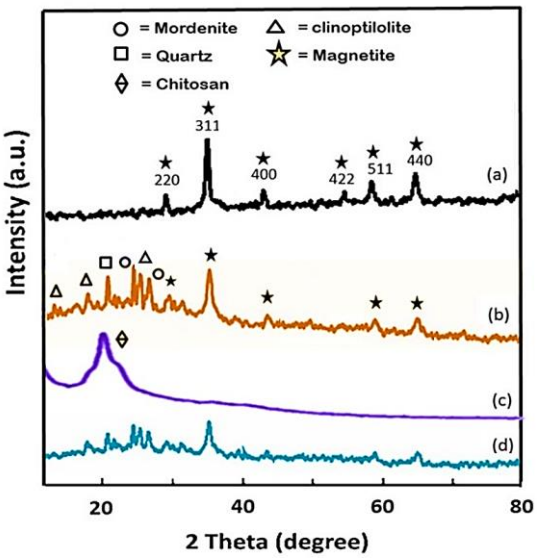

Fig. 1. The XRD patterns of (a) as-synthesized Fe_3O_4, (b) Fe_3O_4@Zeo, (c) chitosan, and (d) Fe_3O_4@Zeo(Chi-Glu-Chi).

The main peaks of Fe_3O_4 are still detected in the diffractogram of Fe_3O_4@Zeo although with low intensities (Figure 1b), indicating that the crystal structure of the material is still preserved. The decrease in intensity and the widening of the Fe_3O_4 peaks are possibly due to the formation of coated phase (zeolite) which reduces the X-ray light reaching to Fe_3O_4 material. The diffractogram also shows some new characteristic peaks that resemble to the peaks of some minerals, namely mordenite (2θ = 25.49°, 26.05°, and 27.61°; ICDD no. 06-0239) [45]; clinoptilolite (2θ = 13.20°, and 19.37°; ICDD no. 47-1870) [46], and quartz (2θ = 20.82°, ICDD no. 46-1045) [47].

In Figure 1c, the diffractogram shows two dilated peaks at 2θ of 10° and 20° (the first peak not be covered fully), which is characteristics to chitosan (ICDD no. 039-1894) [48]. The main peaks of Fe_3O_4@Zeo are still detected in the diffractogram of Fe_3O_4@Zeo(Chi-Glu-Chi) (Figure 1d) although with low intensities. This phenomenon indicates that, in Fe_3O_4@Zeo(Chi-Glu-Chi), the amorphous chitosan–glutaraldehyde system covers the Fe_3O_4@Zeo particles without damaging the composite structure.

FTIR analysis

The FTIR spectra of as-synthesized Fe_3O_4, Fe_3O_4@Zeo, chitosan, and Fe_3O_4@Zeo(Chi-Glu-Chi) are presented in Figure 2. The spectrum of as-synthesized Fe_3O_4 (Figure 2a) shows the peak at 572 cm^{-1} related to the stretching vibration of the Fe–O bond on Fe_3O_4 [37, 49]. The peak at approximately 3482 cm^{-1}, attributed to the stretching vibration of the –OH group on H_2O, is reinforced by the peak at 1635 cm^{-1}, belongs to the bending vibration of H–O–H [50, 51]. The spectrum of Fe_3O_4@Zeo (Figure 2b) shows the new peaks of some functional groups. The peak at approximately 1054 cm^{-1} is referred to the asymmetric stretching vibrations of the Si–OH and Al–OH groups on the $(Si/Al)O_4$ tetrahedral zeolite [37, 52]. Other absorption peaks at 451 and 794 cm^{-1} are associated with the asymmetrical bending and symmetrical stretching of Si–O–Si vibrations in quartz, respectively [50, 53]. Figure 2 shows that the 572 cm^{-1} peak on as-synthesized Fe_3O_4 (Figure 2a) shifts to the 586 cm^{-1} peak on Fe_3O_4@Zeo (Figure 2b), which is accompanied by a decrease in absorbance. These observations can be attributed to the formation of Fe–O–Si and Fe–O–Al bonds on Fe_3O_4@Zeo. Also, it can be attributed to the change in the size of Fe_3O_4 nanoparticles, e.g. from large to small [37].

The spectrum of chitosan (Figure 2c) shows some characteristic peaks. The widened peak at approximately 3440 cm^{-1} is related to the stretching vibration of NH_2 in primary amines and the stretching vibration of –OH in the pyranose ring, whereas the peak at 2877 cm^{-1} is due to the –CH stretching vibrations in the pyranose ring. The peaks at 1651 and 1597 cm^{-1} are associated with the vibrations of –C=O in the $NHCOCH_3$ group, whereas the peak at 1381 cm^{-1} is originated from the bending vibration of $–CH_3$ in the $NHCOCH_3$ group. The peak at 1319 cm^{-1} is associated with the pyranose ring complex vibrations of the NHCO group, whereas the peak at 1157 cm^{-1} comes from the stretching vibration of C–O–C in the glycosidic linkage. The peak at 1087 cm^{-1} is associated with the stretching vibration of C–O in the secondary OH group [54-57]. The 3440 and 1651 cm^{-1} peaks are used to calculate the average DD%, according to Equation (2), giving the DD% of 78.35%. This value is quite close to that reported by several researchers, e.g. 71.02% to 82.20% [58], 87.5% to 93% [59], and 77% to 92% [60].

When glutaraldehyde-crosslinked chitosan interacts with Fe_3O_4@Zeo, no shift in the peak of Fe_3O_4 is observed, indicating that no covalent bond is formed between Fe_3O_4 and chitosan.

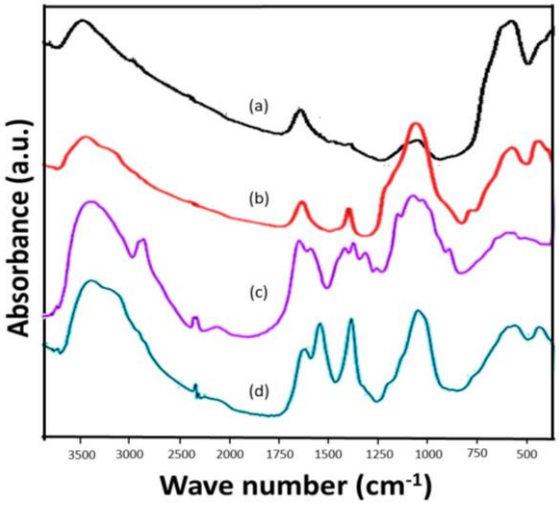

Fig. 2. The FTIR spectra of (a) Fe_3O_4, (b) Fe_3O_4@Zeo, (c) chitosan, and (d) Fe_3O_4@Zeo(Chi-Glu-Chi).

Moreover, no significant shift in the peak of zeolite is detected. The 1072 cm^{-1} peak in Figure 2d is overlapping peaks of 1054 cm^{-1} peak in Figure 2b and the 1087 cm^{-1} peak in Figure 2c. This IR spectra indicate that no covalent bond formed between zeolite and chitosan. However, hydrogen and electrostatic bonds (which cannot be detected by FTIR) are possibly formed. In contrast, changes in other characteristic peaks occur. The 1597 cm^{-1} peak in Figure 2c shifts to the 1556 cm^{-1} peak in Figure 2d, accompanied by the increase in its absorbance. These observations suggest the crosslinking occurrence between the $–NH_2$ group of chitosan and the –C=O group of glutaraldehyde. Moreover, the new characteristic band appears at 1635 cm^{-1}, which is associated with the Schiff base, i.e. the C=N group, resulted from the reaction between the $–NH_2$ group of chitosan and the –C=O group of glutaraldehyde. The band of C-H stretching at wavenumbers of 2700-2800 cm^{-1} and C=O stretching around 1750 cm^{-1} originating from the CHO group in glutaraldehyde, are not observed in Figure 2d. Hence, no free glutaraldehyde is detected, indicating that all glutaraldehydes are involved in cross-linking reaction in the composite [26].

Transmission electron microscopy analysis

Characterization using TEM has been employed to compare the morphology and the particle size. The micrographs are presented in Figure 3. Figure 3a shows the agglomerations of the as-synthesized Fe_3O_4, which can be identified as the formation of dark spheres that widen and stick to one another. This agglomeration is due to the magnetic properties of Fe_3O_4 particles; thus, they tend to attract each other. Figure 3b shows the presence of Fe_3O_4 nanoparticles, which are quite evenly covered by zeolite, indicating that Fe_3O_4 has been successfully coated with zeolite. Figure 3c shows the dispersion of Fe_3O_4@Zeo spheres incorporated in the chitosan–glutaraldehyde system, suggesting the success of the formation of composite materials.

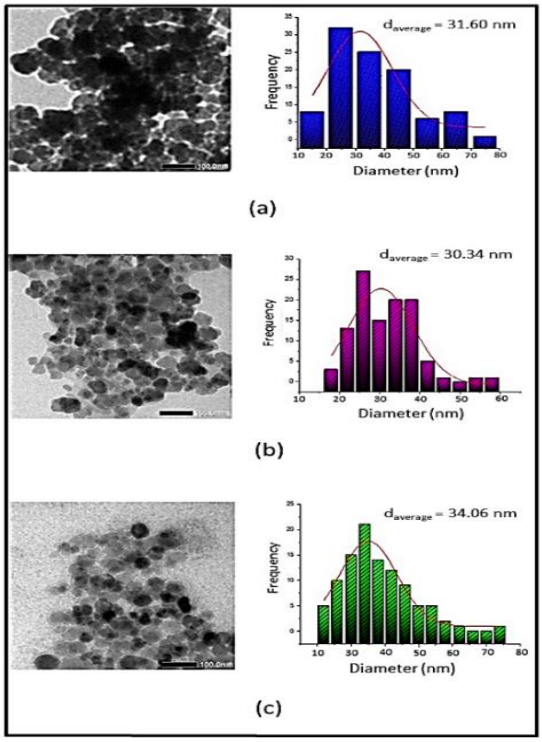

Fig. 3. TEM micrographs and particle size distribution for (a) as-synthesized Fe_3O_4, (b) Fe_3O_4@Zeo, and (c) Fe_3O_4@Zeo(Chi-Glu-Chi).

The distribution of particle size has been determined using the ImageJ software [61]. The results indicate that the average diameter size of as-synthesized Fe_3O_4, Fe_3O_4@Zeo, and Fe_3O_4@Zeo(Chi-Glu-Chi) are 31.60, 30.34, and 34.06 nm, respectively. It is interesting to note that the average diameter of Fe_3O_4@Zeo is smaller than Fe_3O_4 bald. Apparently, the presence of zeolites edict the growth of Fe_3O_4 crystals, making the size of Fe_3O_4 particles in Fe_3O_4@Zeo smaller. This is in accordance with the interpretation of FTIR spectra changes that have been discussed in the previous section. Meanwhile, the average diameter of Fe_3O_4@Zeo(chi-glu-chi) is larger than that of Fe_3O_4@Zeo. This is probably due to the layer of glutaraldehyde crosslinked chitosan.

The Magnetic hysteresis curve

The hysteresis curve provides information about saturation magnetization (M_s), i.e. the saturation point of the material when it was brought closer to the external magnetic field. The increasing magnetic field, which comes in contact with the material, causes the

change in the magnetic moment up to the saturation point. Figure 4 shows the hysteresis curves of as-synthesized Fe_3O_4, Fe_3O_4@Zeo, and Fe_3O_4@Zeo(Chi-Glu-Chi) at room temperature. The figure clearly shows that M_s decreases when Fe_3O_4 is modified with both zeolite and zeolite–chitosan–glutaraldehyde. The M_s values of as-synthesized Fe_3O_4, Fe_3O_4@Zeo, and Fe_3O_4@Zeo(Chi-Glu-Chi) are 55.5, 35.2, and 27.5 emu/g, respectively; which are less than that of bulk Fe_3O_4, i.e. approximately 90 emu/g [61]. The low M_s values of the materials synthesized in this study can be attributed to small crystallite size of Fe_3O_4. Moreover, zeolite and/or chitosan–glutaraldehyde as nonmagnetic materials in Fe_3O_4@Zeo and Fe_3O_4@Zeo(Chi-Glu-Chi) composites can serve as a magnetic shield for Fe_3O_4, resulting in the decrease in their M_s values [62]. Nevertheless, the M_s value of Fe_3O_4@Zeo(Chi-Glu-Chi) of about 27.5 emu/g is still sufficient in practice for the separation of the composites using a permanent magnet [62], as shown in Figure 4 (inset).

By comparing the M_s values of the three materials, it can be estimated that the Fe_3O_4 contents in the Fe_3O_4@Zeo and Fe_3O_4@Zeo(Chi-Glu-Chi) composites are approximately 54.4% and 49.6%, respectively.

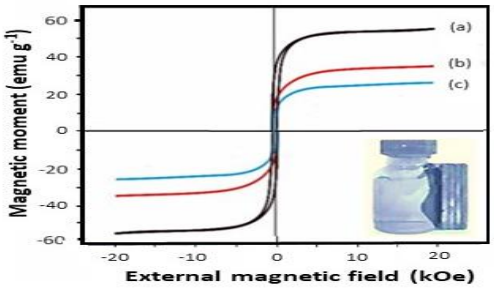

Fig. 4. Magnetic hysteresis curves at room temperature of (a) Fe_3O_4, (b) Fe_3O_4@Zeo, and (c) Fe_3O_4@Zeo(Chi-Glu-Chi). Inset: respond of Fe_3O_4@Zeo(Chi-Glu-Chi) to the magnetic field.

The loops in Figure 4a indicate that the as-synthesized Fe_3O_4 in this study is ferrimagnetic [63], with the remanence of 30.13 emu/g. In the case of Fe_3O_4@Zeo (Figure 4b) and Fe_3O_4@Zeo(Chi-Glu-Chi) (Figure 4c), the curves were S-shaped over the applied magnetic field and did not have loops. Therefore, Fe_3O_4@Zeo and Fe_3O_4@Zeo(Chi-Glu-Chi) are superparamagnetic materials, which only have magnetic properties when they are in a magnetic field [35, 58-62]. The superparamagnetic property of the material allows it to be dispersed with a slight wobble when the magnetic field is removed. This property is very important in adsorption and various other applications [36]. The formation of Fe_3O_4@SiO_2 and Fe_3O_4@Zeo were illustrated in Figure 5. Zeolite on Fe3O4@Zeo interacting with Chi-Glu-Chi via hydrogen bonds to form Fe3O4@Zeo(Chi-Glu-Chi) [15, 64] is illustrated in Figure 6, while the crosslinking of chitosan using glutaraldehyde [65] is illustrated in Figure 7.

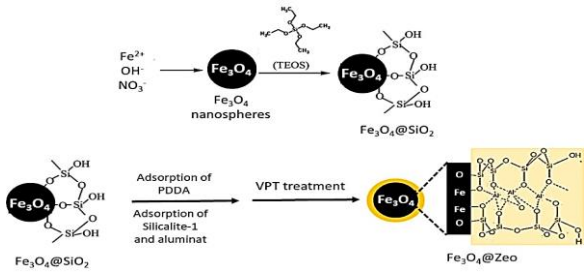

Fig. 5. Scheme formation of Fe_3O_4@SiO_2 and Fe_3O_4@Zeo.

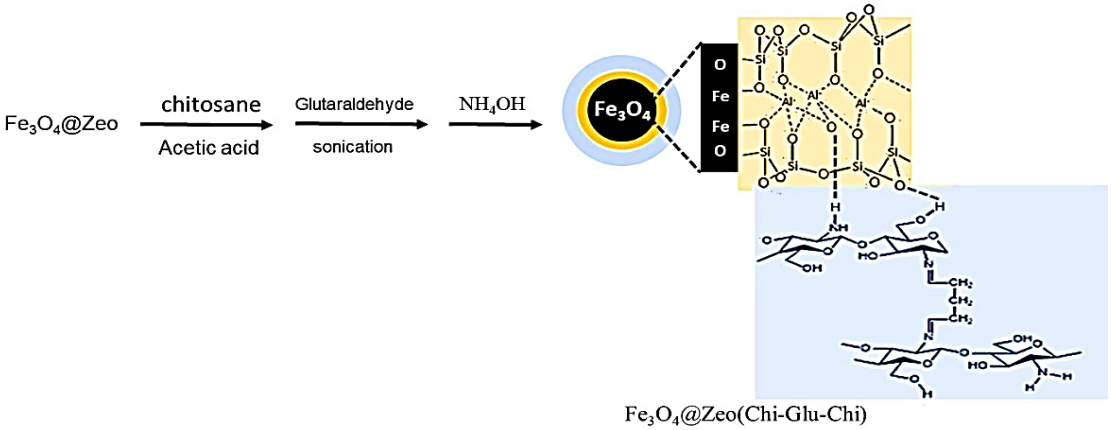

Fig. 6. Scheme formation of Fe_3O_4@Zeo(Chi-Glu-Chi)

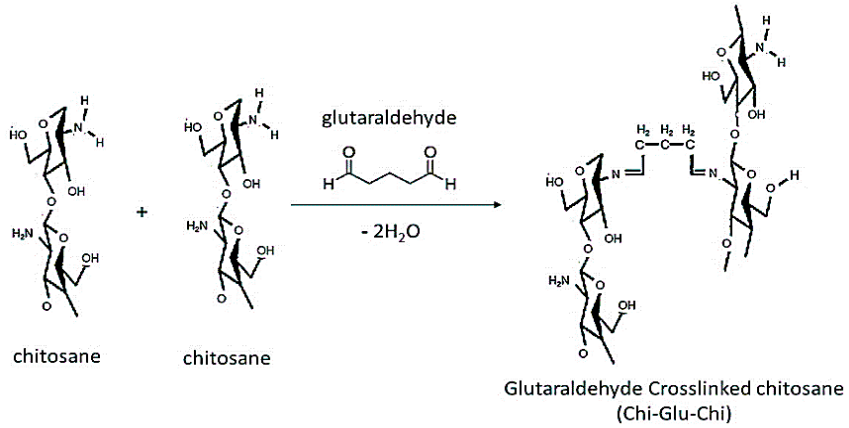

Fig. 7. Crosslinking of chitosan using glutaraldehyde.

.

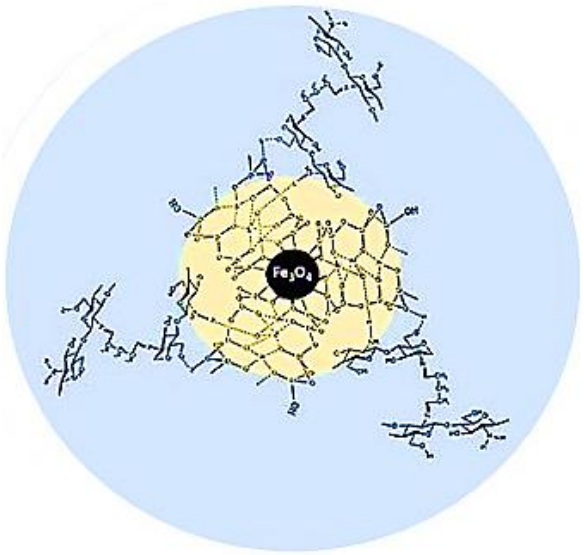

Fig. 8. Hypothetical structure of the Fe_3O_4@Zeo(Chi-Glu-Chi) composite.

The hypothetical structure of Fe_3O_4@Zeo(Chi-Glu-Chi) is illustrated in Figure 8. The hypothetical structure of the composite (Figure 8) shows the existence of active adsorption sites from zeolite and chitosan. Therefore, it is expected that this composites are able to adsorb pollutants through ion exchange mechanisms and/or chelate formation mechanisms. In addition, the magnetite nanoparticles are positioned at the center of the sphere as a core. This makes the magnetite is well protected from oxidation so that their magnetic properties will be longer preserved.

4. Conclusions

The superparamagnetic nanocomposite of Fe3O4@Zeo(Chi-Glu-Chi) has successfully synthesized. The X-ray diffractogram proves that the Fe_3O_4 formed is a cubic and it does not affected by the presence of zeolite and chitosan–glutaraldehyde in the composite. The FTIR spectral analysis has revealed the formation of Fe–O–Al and Fe–O–Si bonds between Fe_3O_4 and zeolite, resulting in the formation of Fe_3O_4@Zeo. Moreover, the crosslinking between $–NH_2$ group of chitosan and –C=O group of glutaraldehyde produces the Schiff base, C=N group. The interaction between Fe_3O_4@Zeo composite and glutaraldehyde-crosslinked chitosan gel system is believed to be occurred via hydrogen bonds. The TEM images confirms that Fe_3O_4@Zeo(Chi-Glu-Chi) consists of Fe_3O_4@Zeo particle spheres incorporated in the glutaraldehyde-crosslinked chitosan gel system. The TEM observations indicates that the diameter size of Fe_3O_4@Zeo(Chi-Glu-Chi) nanocomposites is in the range of 15–75 nm, while the average diameter is 34.06 nm. The VSM study shows that the nanocomposites of Fe_3O_4@Zeo(Chi-Glu-Chi) are superparamagnetic, with a saturation magnetization of 27.5 emu/g. The magnetically separable

nanocomposite synthesized in this study is quite interesting and may be applied in the removal of heavy metals and cationic dyes.

Conflicts of interest

"There are no conflicts to declare".

Acknowledgments

The first author gratefully acknowledges Faculty of Mathematics and Natural Sciences, Universitas Gadjah Mada (UGM) for financial support through BPPTNBH research grant.

.

References

1. Behnajady M.A. and Bimeghdar S., Synthesis of mesoporous NiO nanoparticles and their application in the adsorption of Cr(VI). *Chem. Eng. J.*, 239, 105–113(2014). https://doi.org/10.1016/j.cej.2013.10.102
2. Chen H., Yan T. and Jiang F., Adsorption of Cr(VI) from aqueous solution on mesoporous carbon nitride. *J. Taiwan Inst. Chem. Engrs.*, 45, 1842–1849(2014). https://doi.org/10.1016/j.jtice.2014.03.005
3. Hosny R., Fathy M., Ramzi M., Abdel Moghny Th., Desouky S.E.M. and Shama S.A., Treatment of the oily produced water (OPW) using coagulant mixtures. Egypt. *J. Pet.*, 25(3), 391–396(2016). https://doi.org/10.1016/j.ejpe.2015.09.006
4. Xie J., Li C, Chi L. and Wu D., Chitosan modified zeolite as a versatile adsorbent for the removal of different pollutants from water. *Fuel*, 103, 480–485(2013). https://doi.org/10.1016/j.fuel.2012.05.036
5. Wu F. C., Tseng R. L. and Juang R. S. J., Enhanced abilities of highly swollen chitosan beads for color removal and tyrosinase immobilization. *J. Hazard. Mater*, 81(167), 167–177(2001). http://dx.doi.org/10.1016/S0304-3894(00)00340-X
6. Wang L., Xing R., Liu S., Cai S., Yu H., Feng J., Li R. and Li P., Synthesis and evaluation of a thiourea-modified chitosan derivative applied for adsorption of Hg(II) from synthetic wastewater. *Int. J. Biol. Macromol*., 46(5), 524–528(2010). https://doi.org/10.1016/j.ijbiomac.2010.03.003
7. Tran H. V., Tran L. D. and Nguyen T. N., Preparation of chitosan/Fe_3O_4 composite beads and their application for removal of Pb(II) and Ni(II) from aqueous solution. *Mater. Sci. Eng*., 30(2), 304– 310(2010). https://doi.org/10.1016/j.msec.2009.11.008
8. Wan M. W., Kan C. C., Buenda D. R. and Maria L. P. D., Adsorption of Copper(II) and Lead(II) ions from aqueous solution on chitosan-coated sand. *Carbohydrate Polymers*, 80(3), 891–899(2010). https://doi.org/10.1016/j.carbpol.2009.12.048
9. Kumar M., Muzzarelli R.A.A., Muzzarelli C., Sashiwa H. and Domb A., Chitosan chemistry and pharmaceutical perspectives. *Chem. Rev*., 104(12), 6017–6084(2004). https://doi.org/10.1021/cr030441b
10. Ibrahim, H.M., Mostafa, M. and Kandile, N.G., Potential use of N-carboxyethylchitosan in biomedical applications: Preparation, characterization, biological properties. *Int. J. Biol. Macromol*. 149, 664-671(2020). https://doi.org/10.1016/j.ijbiomac.2020.01.299
11. Ibrahim, H.M., Reda, M.M. and Klingner, A., Preparation and characterization of green carboxymethylchitosan (CMCS) – Polyvinyl alcohol (PVA) electrospun nanofibers containing gold nanoparticles (AuNPs) and its potential use as biomaterials. *Int. J. Biol. Macromol*. 151, 821-829(2020). https://doi.org/10.1016/j.ijbiomac.2020.02.174
12. El-Alfy, E.A., El-Bisi, M.K., Taha, G.M. and Ibrahim, H.M., Preparation of biocompatible chitosan nanoparticles loaded by tetracycline, gentamycin and ciprofloxacin as novel drug delivery system for improvement the antibacterial properties of cellulose based fabrics. *Int. J. Biol. Macromol*. 161, 1247-1260(2020). https://doi.org/10.1016/j.ijbiomac.2020.06.118
13. Ibrahim, H.M., Farid, O.A., Samir, A. and Mosaad, R.M., Preparation of chitosan antioxidant nanoparticles as drug delivery system for enhancing of anti-cancer drug. Key engineering Materials 759, 92-97(2018). https://doi.org/10.4028/www.scientific.net/KEM.759.92
14. Rinaudo M., Pavlov G. and Desbrieres J., Influence of acetic acid concentration on the solubilization of chitosan. *Polymer*, 40(25), 7029–7032(1999). DOI: 10.1016/S0032-3861(99)00056-7

15. Gao Y., Ru Y., Zhou L., Wang X. and Wang J., Preparation and characterization of chitosan-zeolite molecular sieve composite for ammonia and nitrate removal. *Adv. Compos. Lett.*, 27(5), 185–192(2018).
https://journals.sagepub.com/doi/pdf/10.1177/096369351802700502
16. Wan Ngah W.S., Teonga L.C., Toha R.H. and Hanafiah M.A.K.M., Utilization of chitosan–zeolite composite in the removal of Cu(II) from aqueous solution: Adsorption, desorption, and fixed-bed column studies. *Chem. Eng. J.*, 209, 46–53(2012). https://doi.org/10.1016/j.cej.2012.07.116
17. Dragan E.S., Dinu M.V. and Timpu D., Preparation and characterization of novel composites based on chitosan and clinoptilolite with enhanced adsorption properties for Cu^{2+}. Bioresour. *Technol.*, 101(2), 812–817(2010). https://doi.org/10.1016/j.biortech.2009.08.077
18. Dinu M.V. and Dragan E.S., Evaluation of Cu^{2+}, Co^{2+}, and Ni^{2+} ions removal from aqueous solution using a novel chitosan/clinoptilolite composite: Kinetics and isotherms. *Chem. Eng. J.*, 160(1), 157–163(2010).
DOI: 10.1016/j.cej.2010.03.029
19. Djelad A., Morsli A., Robitzer M., Bengueddach A., Renzo F.D. et al., Sorption of Cu(II) Ions on chitosan-zeolite X composites: Impact of Gelling and Drying Conditions. *Molecules*, MDPI, 21, 109(2016). DOI: 10.3390/molecules21010109
20. Baysal K., Aroguz A.Z., Adiguzel Z. and Baysal B.M., Chitosan/alginate crosslinked hydrogels: preparation, characterization, and application for cell growth purposes. *Int. J. Biol. Macromol.*, 59, 342-348(2013). https://doi.org/10.1016/j.ijbiomac.2013.04.073
21. Shaheen S.M., Derbalah A.S. and Moghanm F.S., Removal of heavy metals from aqueous solution by zeolite in competitive sorption system, *IJESD*, 3(4), 362-367(2012). DOI:10.7763/IJESD.2012.V3.248
22. Safarik I., Horska K., Pospiskova K. and Safarikova M., Magnetically responsive activated carbons for bio - and environmental applications. *IRECHE*, 4(3), 346–352(2012). https://pdfs.semanticscholar.org/1642/537503a8857c96529c0453a358a662b0370f.pdf
23. Nyankson E., Adjasoo J., Efavi J.K., Amedalor R., Yaya A., Manu G.P., Asare K. and Amartey N.A., characterization and evaluation of zeolite A/Fe_3O_4 nanocomposite as a potential adsorbent for removal of organic molecules from wastewater. *jchem*, 2019, 1-13(2019). https://doi.org/10.1155/2019/8090756
24. Pylypchuk I.V., Kołodyńska D., Kozioł M. and Gorbyk1 P.P., Gd-DTPA Adsorption on chitosan/Fe_3O_4 nanocomposites. Nanoscale Res. Lett., 11, 168(2016). DOI: 10.1186/s11671-016-1363-3
25. Hong M, Yu L., Wang Y., Zhang J, Chen Z., Dong L. andLi R., Heavy metal adsorption with zeolites: The role of hierarchical pore architecture. *Chem. Eng. J.*, 359, 363-372(2019). https://doi.org/10.1016/j.cej.2018.11.087
26. Truong T.T.C., Takaomi K. and Bui H.M., Chitosan/zeolite composite membranes for the elimination of trace metal ions in the evacuation permeability process. *J. Serbian Chem. Soc*., 84 (1), 83–97(2019).
https://doi.org/10.2298/JSC180606085T
27. Gao Y. and Zhang J., Chitosan modified zeolite molecular sieve particles as a filter for ammonium nitrogen removal from water. *Int. J. Mol. Sci.*, 21(7), 2383(2020). https://doi.org/10.3390/ijms21072383
28. Wan Ngah W. S., Teong L. C. , Wong C. S. and Hanafiah M. A. K. M., Preparation and characterization of chitosan-zeolite composites. *J. Appl. Polym. Sci.*, 125, 2417–2425(2012). https://doi.org/10.1002/app.36503
29. Barbosa G.P., Debone H.S., Severino P., Souto E.B., da Silva C.F., Design and Characterization of Chitosan/Zeolite Composite Films - Effect of zeolite type and zeolite dose on the film properties. *Mater. Sci. Eng.: C*, 60, 246–254(2016).
https://doi.org/10.1016/j.msec.2015.11.034
30. McCarty K.F., Monti M., Nie S., Siegel D.A., Starodub E., Gabaly F.E., McDaniel A.H., Shavorskiy A., Tyliszczak T., Bluhm H., Bartelt N.C., and Figuera J., Oxidation of Magnetite(100) to Hematite Observed by in Situ Spectroscopy and Microscopy. *J. Phys. Chem. C*, 118(34), 19768–19777(2014). https://doi.org/10.1021/jp5037603
31. Schwaminger S. P., Bauer D., Fraga-García P., Wagnerb F. E., and Berensmeier S., Oxidation of magnetite nanoparticles: impact on surface and crystal properties. *CrystEngComm*, 19, 246-255(2017). https://doi.org/10.1039/C6CE02421A
32. El-Din T.A.S., Elzatahry A.A., Aldhayan D.M., Al-Enizi, A.M. and Al-Deyab S.S., Synthesis and Characterization of Magnetite

Zeolite Nano Composite. *Int. J. Electrochem. Sci.*, 6 (2011) 6177 – 6183. https://www.researchgate.net/publication/265806262_Synthesis_and_Characterization_of_Magnetite_Zeolite_Nano_Composite

33. Andrade Â.L., Cavalcante, L.C.D., Fabris, J.D. et al. Zeolite-magnetite composites to remove Hg^{2+} from water. *Hyperfine Interact* 240, 83 (2019). https://doi.org/10.1007/s10751-019-1624-5
34. Ahmadi E., Kakavandi, B., Azari, A., Izanloo, H., Gharibi, H., Mahvi, A.H., Javid, A., and Hashemi, S.Y., The performance of mesoporous magnetite zeolite nanocomposite in removing dimethyl phthalate from aquatic environments, *DESALIN WATER TREAT*, 57(57), 27768-27782(2016). DOI: 10.1080/19443994.2016.1178174
35. Faghihian H., Moayed M., Firooza A., Iravani M., Evaluation of a new magnetic zeolite composite for removal of Cs^{+} and Sr^{2+} from aqueous solutions: Kinetic, equilibrium and thermodynamic studies. *C R Chim*, 17(2), 108–117(2014). https://doi.org/10.1016/j.crci.2013.02.006
36. Deng Y., Deng C., Qi D., Liu C., Liu J., Zhang X., and Zhao D., Synthesis of core/shell colloidal magnetic zeolite microspheres for the immobilization of trypsin, *Adv. Mater*. 21, 1377–1382(2009).
37. Gaffer A., Amal A, Kahlawy A. and Aman D., Magnetic zeolite-natural polymer composite for adsorption of chromium(VI). *Egypt. J. Pet.*, 26(4), 995–999(2017). https://doi.org/10.1016/j.ejpe.2016.12.001
38. Nyiro-Kosa I., Recnik A., Posfai M., Novel methods for the synthesis of magnetite nanoparticles with special morphologies and textured assemblages. *J. Nanoparticle Res*. 14, 1150(2012). DOI: 10.1007/s11051-012-1150-8
39. Dai C., Li J., Zhang A., Nie C., Song C., and Guo X, Precise control of the size of zeolite B-ZSM-5 based on seed surface crystallization. *RSC Adv.***, 7**, 37915–37922(2017). https://doi.org/10.1039/C6RA28030G
40. Xu X., Deng C. H., Gao M., Yu W., Yang P., Zhang X., Synthesis of magnetic microspheres with immobilized metal ions for enrichment and direct determination of phosphopeptides by matrix- assisted laser desorption ionization mass spectrometry. *Adv. Mater*. 18, 3289(2006). DOI:10.1002/ADMA.200601546
41. Ozdemir O.D. and Pişkin S., Zeolite X, Synthesis with Different Sources. *IJCEBS*, 1, 2 (2013). http://www.isaet.org/images/extraimages/D313094.pdf
42. Dewi C., Mudjijono H., and Angwar M., Isolation and characterization of chitin and chitosan prepared under various processing times, Indones. *J. Chem.*, 8 (2), 189–192(2008). DOI: 10.22146/ijc.21635
43. Kasaai M.R., A review of several reported procedures to determine the degree of N-acetylation for chitin and chitosan using infrared spectroscopy. *Carbohydr. Polym*., 71(4), 497–508(2008). https://doi.org/10.1016/j.carbpol.2007.07.009
44. Silva V.A.J., Andrade P.L., Silva M.P.C., Bustamante D. A., Valladares L.L.S., Aguiar J.A., Synthesis and characterization of Fe_3O_4 nanoparticles coated with fucan polysaccharides. *J. Magn. Magn. Mater*., 343, 138-143(2013). https://doi.org/10.1016/j.jmmm.2013.04.062
45. A. Mustain, G.Wibawa, M. F. Nais, M. Falah, Synthesis of zeolite NaA from low grade (high impurities) Indonesian natural zeolite, Indo. J. Chem. 14(2) (2014) 138 – 142. DOI:10.22146/ijc.21250.
46. P. Miądlicki, A. Wróblewska, K. Kiełbasa, Z. C. Koren, B. Michalkiewicz, Sulfuric acid modified clinoptilolite as a solid green catalyst for solvent-free α-pinene isomerization process, MICROPOR MESOPOR MAT, 324 (2021) 111266. https://doi.org/10.1016/j.micromeso.2021.111266.
47. Xue S.H, Xie H., Ping H., Li Q.C., Su B.L., Fu Z.Y., Induced Transformation of Amorphous Silica to Cristobalite on Bacterial Surface. *RSC Adv.*, 5, 71844-71848(2015). https://doi.org/10.1039/C5RA13619A
48. Abdel-Moneim A., El-Shahawy A., Yousef A.I., El-Twab S.M.A., Elden Z.E., Taha M., Novel polydatin-loaded chitosan nanoparticles for safe and efficient type 2 diabetes therapy: *In silico, in vitro* and *in vivo* approaches. *Int. J. Biol. Macromol*., 154, 1496-1504(2020). https://doi.org/10.1016/j.ijbiomac.2019.11.031
49. Petcharoen A. and Sirivat A., Synthesis and characterization of Fe_3O_4 nanoparticles via the

chemical co-precipitation method. *Mater. Sci. Eng.: B*, 177(5), 421–427(2012). DOI: 10.1016/j.mseb.2012.01.003.

50. Orha C., Pop A., Lazau C., Grozescu L., Tiponut V. and Manea, F., Structural and sorption properties of copper doped natural and synthetic zeolite. *Environ Eng Manag J*, 11, 641(2012). DOI: 10.1109/SMICND.2011.6095797
51. Medina A., Gamero P. and Querol X. et al., Fly ash from Mexican mineral coal I: Mineralogical and chemical characterization. *J. Hazard. Mater.*, 181(1–3), 82–90(2010). https://doi.org/10.1016/j.jhazmat.2010.04.096
52. Neyaz N., Zarger M.S.S. and Siddiqui W.A., Synthesis and characterization of modified Fe_3O_4 superparamagnetic nanocomposite for removal of toxic metals from groundwater. *Int. J. Environ. Sci.*, 5(2), 260–269(2014). DOI: 10.6088/ijes.2014050100022
53. Saikia B.J., Parthasarathy G., Borah R.R. and Borthakur R., Raman and FTIR spectroscopic evaluation of clay minerals and estimation of metal contaminations in natural deposition of surface sediments from Brahmaputra River. *IJG*, 7(7), 873–883(2016). http://dx.doi.org/10.4236/ijg.2016.77064
54. Ramya R., Sudha P.N., Mahalakshmi J., Preparation and characterization of chitosan binary blend. IJSRP, 2(10), 1–9(2012). http://www.ijsrp.org/research-paper-1012/ijsrp-p1011.pdf
55. Govindan S., Nivethaa E.A.K., Saravanan R., Narayanan V. and Stephen A., Synthesis and characterization of chitosan–silver nanocomposite. *Appl. Nanosci.*, 2, 299–303(2012). https://doi.org/10.1007/s13204-012-0109-5
56. Badawy R. M. and Mohamed H. I., Chitin extraction, composition of different six insect species and their comparable characteristics with that of the shrimp. *Am. J. Sci.*, 11(6), 127–134(2015). http://www.jofamericanscience.org
57. El Knidri H., Belaabed R., El khalfaouy R., Laajeb A., Addaou A. and Lahsini A., Physicochemical characterization of chitin and chitosan produced from Parapenaeus Longirostris shrimp shell wastes. *J. Mech. Eng. Sci.*, 8(10), 3648–3653(2017). http://www.jmaterenvironsci.com/
58. Nouri M., Khodaiyan F., Razavi S.H., and Mousavi M., Improvement of chitosan production from Persian Gulf shrimp waste by response surface technology. *Food Hydrocoll.*, 59, 50–58(2016). https://doi.org/10.1016/j.foodhyd.2015.08.027
59. Alishahi A., Mirvaghefi A. and Tehrani M.R. *et al*., Enhancement and characterization of chitosan extraction from the wastes of shrimp packaging plants. *J POLYM ENVIRON*, 19, 776–783(2011). https://doi.org/10.1007/s10924-011-0321-5
60. El-Nesr E. M., Raafat A. I., Nasef Sh. M., Soliman E. A. and Hegazy1 E.A., Chitin and chitosan extracted from irradiated and non-irradiated shrimp wastes (comparative analysis study). *AJNSA*, 46(1), 53–66(2013). http://www.esnsa-eg.com/download/researchFiles/_5_%2064.pdf
61. Abramoff M.D., Magalhaes P.J. and Ram S.J., Image processing with Image. *Biophotonics Int.*, 11(7), 36-42(2004). http://dspace.library.uu.nl/handle/1874/204900
62. Ozel F. and Kockar H., Growth and characterizations of magnetic nanoparticles under hydrothermal conditions: Reaction time and temperature. *J. Magn. Magn. Mater*., 373, 213–216(2015). https://doi.org/10.1016/j.jmmm.2014.02.072
63. Baumgartner J., Bertinetti L., Widdrat M., Hirt A.M. and Faivre D., Formation of Fe_3O_4 nanoparticles at low temperature: from superparamagnetic to stable single domain particles. *PLoS One*, 8(3), 1–6(2013). DOI:10.1371/journal.pone.0057070
64. Jawad A.H., Abdulhameed, A.S., Reghioua, A., Yaseen, Z.M., Zwitterion composite chitosan-epichlorohydrin/zeolite for adsorption of methylene blue and reactive red 120 dyes. *Int. J. Biol. Macromol.*, 163, 756-765(2020). https://doi.org/10.1016/j.ijbiomac.2020.07.014
65. Islam N., Wang H., Maqbool F., and Ferro V., In Vitro Enzymatic Digestibility of Glutaraldehyde-Crosslinked Chitosan Nanoparticles in Lysozyme Solution and Their Applicability in Pulmonary Drug Delivery. *Molecules*, *24*(7),1271(2019). https://doi.org/10.3390/molecules24071271